Friction spot extrusion welding on dissimilar materials AA2024-T3 to AA5754-O: Effect of shoulder plunge depth

S. Memon[1], M. Paidar[2*], K. P. Mehta[3,4], B. Babaei[5], H. M. Lankarani[1]

[1]*Department of Mechanical Engineering, Wichita State University, Wichita, KS, 67260-133, USA*

[2]*Department of Materials Engineering, South Tehran Branch, Islamic Azad University, Tehran, Iran*

[3]*Advanced Manufacturing and Materials Research Group, Department of Mechanical Engineering, School of Engineering, Aalto University, Helsinki, Finland*

[4]*Department of Mechanical Engineering, School of Technology, Pandit Deendayal Petroleum University, Gandhinagar, Gujarat, India*

[5]*School of Mechanical and Manufacturing Engineering, University of New South Wales, Sydney, NSW, 2052, Australia*

[*] Corresponding author Email: m.paidar@srbiau.ac.ir

Abstract

In the present investigation, friction spot extrusion welding was investigated for dissimilar AA2024-T3 and AA5754-O materials, under the effect of three different shoulder plunge depths of 0.25, 0.35 and 0.45 mm, keeping other parameters constant. The welded specimens were evaluated by visual inspection, optical microscopy, scanning electron microscopy, electron backscattered diffractions, and tensile testing. The results revealed that the effective metallurgical bonding and mechanical locking were obtained in case of weld produced by plunge depth of 0.45 mm. The metallurgical bonding is obtained between extruded material and surfaces of predrilled cavity, whereas mechanical locking is obtained through filling an extruded material in the predrilled cavity. The plunge depth variations influence the grain structures of processed zones. Increased plunge depth of 0.45 mm results in effective materials mixing with zigzag pattern of oxide layer mixed in the stir zone. In case of weld produced by plunge depth of 0.25 mm, the oxide layer was found as separating layer between workpieces. The weld produced by maximum plunge depth of 0.45 mm was resulted to higher fracture load of 5198 N. Trans-granular ductile fracture was observed for weld produced by plunge depth of 0.45 mm.

Keywords: Dissimilar joints, Friction spot extrusion, Friction stir, Plunge depth, Welding.

This is a peer-reviewed, accepted author manuscript of the following research article:
Memon, S., Paidar, M., Mehta, K. P., Babaei, B., & Lankarani, H. M. (2021). Friction Spot Extrusion Welding on Dissimilar Materials AA2024-T3 to AA5754-O: Effect of Shoulder Plunge Depth. Journal of Materials Engineering and Performance, 30(1), 334-345. https://doi.org/10.1007/s11665-020-05387-4

1. Introduction

Manufacturing of lightweight components is an active area of interest for the transport industries such as automotive, aerospace, shipbuilding and railways [1,2]. The joining of dissimilar materials is considered as the lightweight structural solution [3–5]. Friction-based welding is applied to obtain different dissimilar joints due to its number of advantages [1,4,6–9]. Friction stir spot welding (FSSW) is evolved as an effective solution from the category of friction-based welding, which is used in case of spot welds [2,10,11]. However, FSSW produces exit hole at the end of retraction phase, wherein the exit hole cavity is left as a volumetric defect, and subsequently that acts as stress concentration location [12]. This exit hole either can be removed by run on and run off tabs or repaired by number of processes such as repairing using probe-less tools [13], consumable bit/tools [14,15], refill friction stir spot welding set-up [16–18], modified friction stir clinching [19–22], and friction stir spot extrusion welding [23]/dieless friction stir extrusion joining [24–26]. These processes are operated under the process principle of friction-based welding and joining, wherein viscoplastic behavior of material is governed to repair or heal the exit hole at the area of joint.

Different aluminum alloys are increasingly applied to manufacture various components of transport industries, wherein welding of similar and dissimilar aluminum alloys are performed [1,3,10]. As mentioned, friction-based welding is one of the best manufacturing categories for similar and dissimilar aluminum alloys. FSSW is explored for different combinations of aluminum alloy welding such as AA7075 to AA2024 [27], AA5754 to AA6061 [28], AA5754 to AA6082 [29], AA2024 to AA6061 [30] and AA5754 to AA2024 [31]. Besides, friction spot extrusion welding is relatively new process and limitedly explored, wherein the exithole effect is greatly eliminated. In friction spot extrusion welding, the joining is obtained in lap joint configuration, wherein the joining is performed by extruded material in the predrilled cavity

from one workpiece to another workpiece. Probe-less tool consisting of flat shoulder surface is applied with adequate forging action to produce material extrusion within intended spot. The friction spot extruded joining is performed using die that creates locking head [32]. Besides, the locking head is eliminated, but strong metallurgical bond is created between extruded material and predrilled surfaces of workpiece in case of dieless friction stir extrusion joining [24–26]. Saju and Narayanan [25] performed dieless friction stir lap joining by extrusion for dissimilar AA5050-H32 and AA6061-T6, using different diameters of pre-drilled holes. They claimed that optimum predrilled diameter is required to obtain sound joint with enhanced mechanical locking and metallurgical bonding. Saju et al. [26] investigated effect of tool's shoulder diameter on joint formation for dissimilar AA5050-H32 and AA6061-T6 joints in case of dieless friction stir extrusion joining. They mentioned that shoulder diameter influences heat flux and extent of plastic deformation of material that subsequently governs the joint formation. Saju and Narayanan [24] studied effect of plunge depth on joining characteristics for dieless friction stir extrusion of dissimilar AA 5052-H32 and AA 6061-T6 materials. They found that increased plunge depth results into better bonding strength. Han et al. [23] investigated flat and scrolled shoulder features in case of friction spot extrusion welding for dissimilar materials of AA2024-T3 and AA6061-T6. They found that scroll shoulder is effective as compared to flat shoulder, in terms of the material flow and sound weld formation.

Friction spot extrusion welding is new process to obtain spot welding. Limited research work is report in the literature for friction spot extrusion welding. Friction stir spot welding is not researched for dissimilar materials AA2024-T3 and AA5754-O, to the best of authors' knowledge. Additionally, the parametric investigation on effect of plunge depth (penetration depth) on friciton sopt extrusion welding for AA2024-T3 and AA5754-O is not investigated hitherto. Therefore, it is worth to investigate effect of plunge depth in case of friction spot extrusion welding for dissimilar joints of AA2024-T3 and AA5754-O materials. In the present

investigation, the study is carried out with friction spot extrusion welding with three different plunge depths of 0.25, 0.35 and 0.45 mm, keeping AA2024-T3 material on top of predrilled AA5754-O material.

2. Experimental details

Dissimilar materials of AA2024-T3 (1.6 mm thickness) and AA5754-O (1.5 mm thickness) were used as base materials in the present investigation. The chemical compositions and mechanical properties of the base materials are shown in Table 1 and Table 2 respectively. The predrilling was performed on AA5754-O material, keeping 3 mm of hole diameter for all the experiments, as shown in Fig: 1 (a). The predrilled diameter is considered from Saju et al. [25] The probe-less tool consists of flat shoulder surface was rotated and plunged into the workpiece with specified plunge depth [as can be seen from Figs: 1 (a) and (b)]. The plunging is limited to top workpiece material.

Table 1. Chemical compositions of base materials (wt.%)

Alloy	Al	Mg	Cu	Cr	Fe	Mn	Si
AA2024-T3	Base	1.28	4.90	0.012	0.44	0.62	0.08
AA5754-O	Base	3.17	0.02	0.037	0.26	0.03	0.61

Table 2. Mechanical properties of the base materials

Alloy	Ultimate Tensile Strength [MPa]	Yield Strength [MPa]	Elongation)%(
AA2024-T3	448	317	14
AA5754-O	217	196	15

. In friction spot extrusion welding (FSEW), the predrilling was provide so that the plastically deformed material flows into it during plunging phase. In the present investigation, the plastically deformed material from AA2024-T3 workpiece flows into predrilled cavity of AA5754-O that in turn results into joint formation by mechanical interlocking and metallurgical bonding between wall of predrilled cavity and extruded material. During experiments, AA2024-T3 material was kept on top of AA5754-O material as shown in Fig: 1

(d). FSEW was performed with constant processing parameters of tool rotation speed, rate of plunging and dwell time, such as rotation speed of 900 rpm, plunging rate of 0.2 mm/min and dwell time of 8 seconds. In FSEW, after the intended plunge depth was obtained, the tool was kept on hold at the same location for dwell time of 8 seconds, in order to obtain bonding between extruded material and predrilled cavity surfaces. Besides, three different plunge depths such as 0.25 mm, 0.35 mm and 0.45 mm were varied. With the same processing parameteric combination, at least five specimens were created to check the repeatability. These specimens are further utilized for testing and characterizations in order to assess the joint characteristics. Three specimens were subjected to tensile testing, whereas rest of the two specimens were subjected to macrograph and microstructure analysis. The probe-less tool consists of 15 mm of shoulder diameter and tool material of H13 tool steel was used in the experimentation. CNC milling machine was utilized to perform FSEW process.

After the processing of FSEW, the joint specimens were subjected to visual inspection of surface crown appearance and flash formation inspection, macrograph analysis of extruded material in the cavity and indentation on top surface of workpiece, optical microscopy, scanning electron microscopy (SEM), energy backscatter diffractions (EBSD), tensile testing and fractured surface inspection of fractured tensile specimens. Macrographs and microscopic analysis were performed on cross-sectional surface of specimens. The cross section of the specimen was obtained through cutting the samples from the center of the shoulder's indentation. Standard metallographic procedure of grinding, polishing and etching (using Baker agent for 110 s and 20 V) were carried out for macrograph and microstructure analysis. The specimens were mechanically polished for subsequent SEM and EBSD analysis. The tensile testing was performed using Instron 5500R machine as shown in Fig: 1 (c), wherein the crosshead speed of 2 mm/min was kept constant. After the tensile testing, the fractured surface analysis was performed using SEM images.

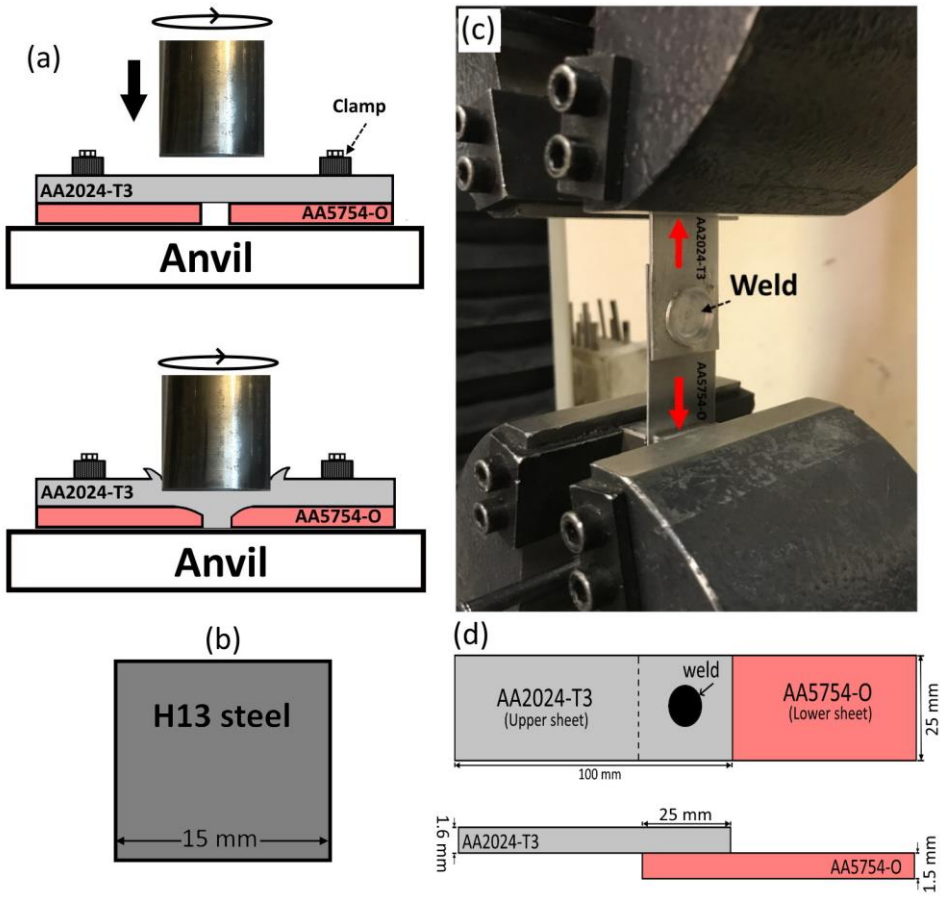

Fig. 1. Schematic of the (a) friction stir extrusion welding process, (b) tool used during process, (c) tensile testing, (d) tensile/shear samples.

3. Results and discussion

The results and discussion are presented in three different subsections such as visual inspection and macrographs, microstructure analysis, and tensile testing.

3.1 Visual inspection and macrographs

Visual inspection of surface crown morphology for welded specimens is carried out. Fig: 2 shows surface morphology of welded specimens made by three different tool penetration depths such as (a) 0.25 mm, (b) 0.35 mm and (c) 0.45 mm. It can be seen that the flash formation increases as the penetration depth increases. In case of weld made by 0.45 mm penetration depth (i.e. highest among three investigated), the maximum flash formation was observed. Additionally, increased indentation depth was observed with an increase in the plunge depth. It is known that the flash formation is depended on heat input conditions and plunge depth [33].

Increase in plunge depth increases axial pressure on plasticized material in the vicinity of thermo-mechanical processing, in case of FSEW. This in turn leads to higher indentation, which subsequently results into displacement of plasticized softened material from processing region to outside of the shoulder's surface and results into flash formation. In the present investigation, the maximum indentation resulted is observed in case of 0.45 mm penetration depth, that can be further tackled with mechanical grinding. The cavity of exit-hole in case of FSSW is through thickness cavity, whereas the cavity of shoulder's indentation is limited to plunging depth in case of FSEW, therefore FSEW cavity can be repaired or grinded more easily as compared to exit hole cavity of FSSW.

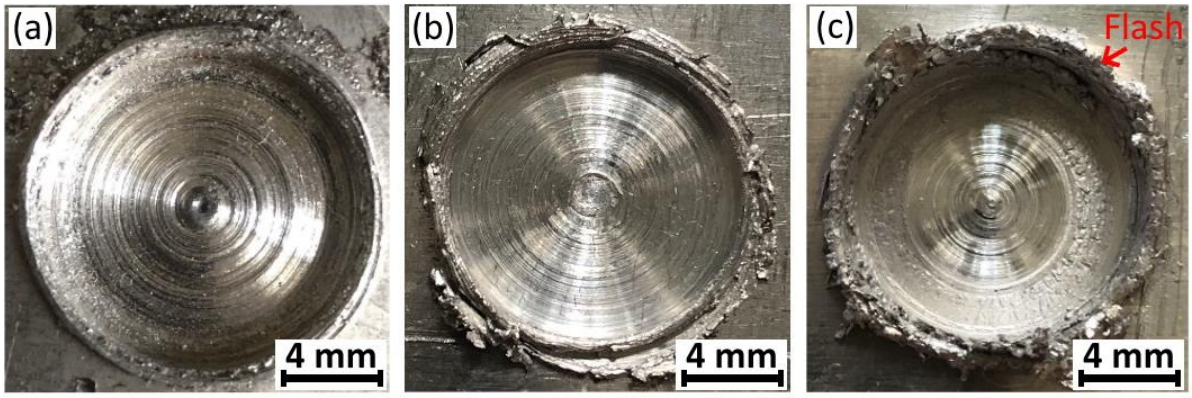

Fig. 2. Surface appearance of welded samples at various tool penetration depths, (a) 0.25 mm, (b) 0.35 mm and (c) 0.45 mm.

Fig: 3 shows cross sectional view of three welds made with tool penetration depths of (a) 0.25 mm, (b) 0.35 mm and (c) 0.45 mm. From these macrographs in Fig: 3, the increase in indentation with increased penetration depths can be confirmed. It can also be seen that the distinct interface between both the materials of AA2024-T3 and AA5754-O was observed as separating line (Fig: 3 (a)), in case of lowest penetration depth of 0.25 mm. However, the predrilled cavity of AA5754-O was filled by extruded material from AA2024-T3 that has created mechanical interlocking. The identified separating line can be predicted as oxide layer formation, as aluminum alloys are prone to form Al_2O_3 at an elevated temperature . No such

oxide layer was detected from other two macrographs of 0.35 mm and 0.45 mm penetration depths (Fig: 3 (b) & (c)). The smaller plunge depth of 0.25 mm may have resulted in inadequate forging force and improper vertical material movement with limited stirring-plunging effect. Besides, increased plunge depths of 0.35 mm and 0.45 mm may have provided enough forging force and effective material movement with enhanced stirring-plunging effect. Therefore, the oxide layer was remained at the interface of both the base materials in case of plunge depth of 0.25 mm, possibly due to inadequate forging force, vertical material flow and stirring-plunging effect. Whereas, enhanced forging force, better vertical material flow and stirring-plunging effect help to break the oxide layer and subsequently broken oxide layer may have stirred and mixed into the extruded material. In case of friction stir welding of aluminum alloys, the enhanced stirring-mixing of oxide layer within the stir zone was observed (as mainly like zigzag pattern), due to strong stirring-mixing effect [34,35].

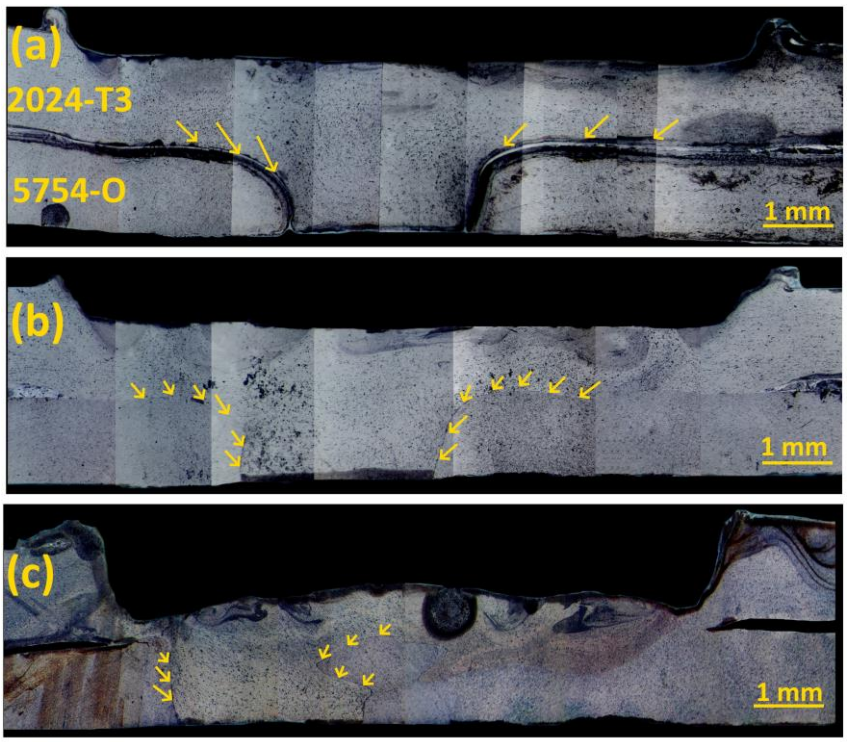

Fig. 3. Macrographs of welds produced as function of tool penetration depth, (a) 0.25 mm, (b) 0.35 mm and (c) 0.45 mm.

3.2 Microstructure analysis

Optical microscopy was performed to analyze microstructures of different processed regions. Fig: 4, Fig: 5 and Fig: 6 show microstructural images of different processed zones for the welds produced by penetration depths of 0.25 mm, 0.35 mm and 0.45 mm respectively. In the processing technique of FSEW, the stirring action was induced by shoulder's surface that is limited to top layer of the cross section due to application of probe-less tool , that in turn resulted with two different microstructures such as stir zone (SZ) and annular stir zone (ASZ). The predrilled cavity was filled by extruded material, which is resulted into extruded zone or plastically deformed zone (PDZ). Besides of these zones, thermo-mechanically affected zone (TMAZ) and heat affected zone (HAZ) are also formed within the cross section progressively from extruded zone to the base material respectively.

Fig: 4 (b) shows microstructures formed as ASZ, flash formation and SZ region, which were influenced by shoulder's surface during stirring and plunging of shoulder. Fig: 4 (c) is higher magnification image of flash formation zone, wherein some of the grains are oriented towards vertical material movement in the direction of flash, and rest of the grains are in horizontal direction. Fig: 4 (d) shows microstructure of ASZ and SZ, where the stirring effect resulted into grain refinement. Grain refinement of SZ can also be evidenced from Fig: 4 (e) at the region shown just below the ASZ. However, in ASZ, the grains seems to be more refined as compared to SZ. The PDZ is shown in Fig: 4 (g) and (i), wherein elongated grains can be observed with larger size as compared to SZ and PDZ. These grains are elongated in the direction of materials' movement towards the predrilled cavity, because of extrusion phenomenon from top workpiece to bottom workpiece. These grains are recrystallized after plastic deformation. Fig: 4 (f) shows microstructure of region below the SZ and above the interface between both the workpiece materials, where horizontally directed grains can be observed that are similar to microstructure of the base material like Fig: 4 (j). Fig: 4 (h) shows

TMAZ, where no major difference in grains was observed as compared to the microstructure of the base material. Additionally, it can be confirmed from Fig: 4 that the mechanical interlocking was obtained with plunge depth of 0.25 mm using FSEW processing. However, effective metallurgical bonding was not established with plunge depth of 0.25 mm, due to interference of oxide layer and inadequate plunge depth (i.e. smaller plunge depth).

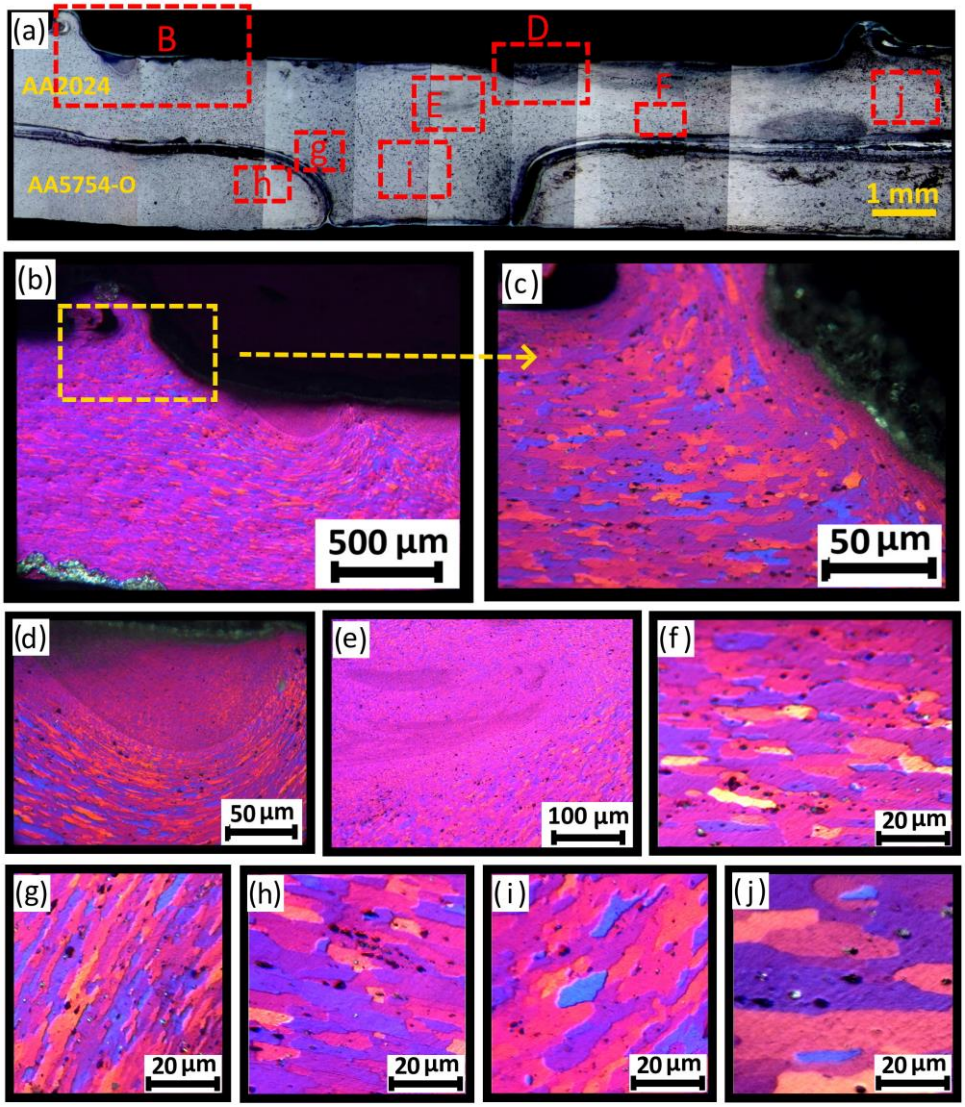

Fig. 4. Optical microstructure images of weld produced by plunge depth of 0.25 mm.

Fig: 5 shows microstructure images of weld produced by plunge depth of 0.35 mm. It can be seen that the indentation on top workpiece was larger than weld of plunge depth 0.25 mm. The metallurgical bonding between extruded material from AA2024-T3 and surface of predrilled cavity of material AA5754-O was obtained effectively as compared the weld of plunge depth

0.25 mm. No distinct oxide layer between workpieces was observed. Fig: 5 (b) shows microstructure image of indentation, flash formation and SZ region, where similar type of grains are observed as seen in case of Fig: 4 (b). Grain refinement can be observed from Fig: 5 (c) for ASZ and SZ, similarly as discussed in case of previous weld of 0.25 mm plunge depth as shown in Fig: 4 (d). Improved material mixing can be observed from Fig: 5 (d) as compared to previous weld shown in Fig: 4. However, thin line was also observed between both the workpieces. However, this thin line (probably of oxide layer) was observed at the interface between extruded zone and predrilled cavity of both the workpieces.

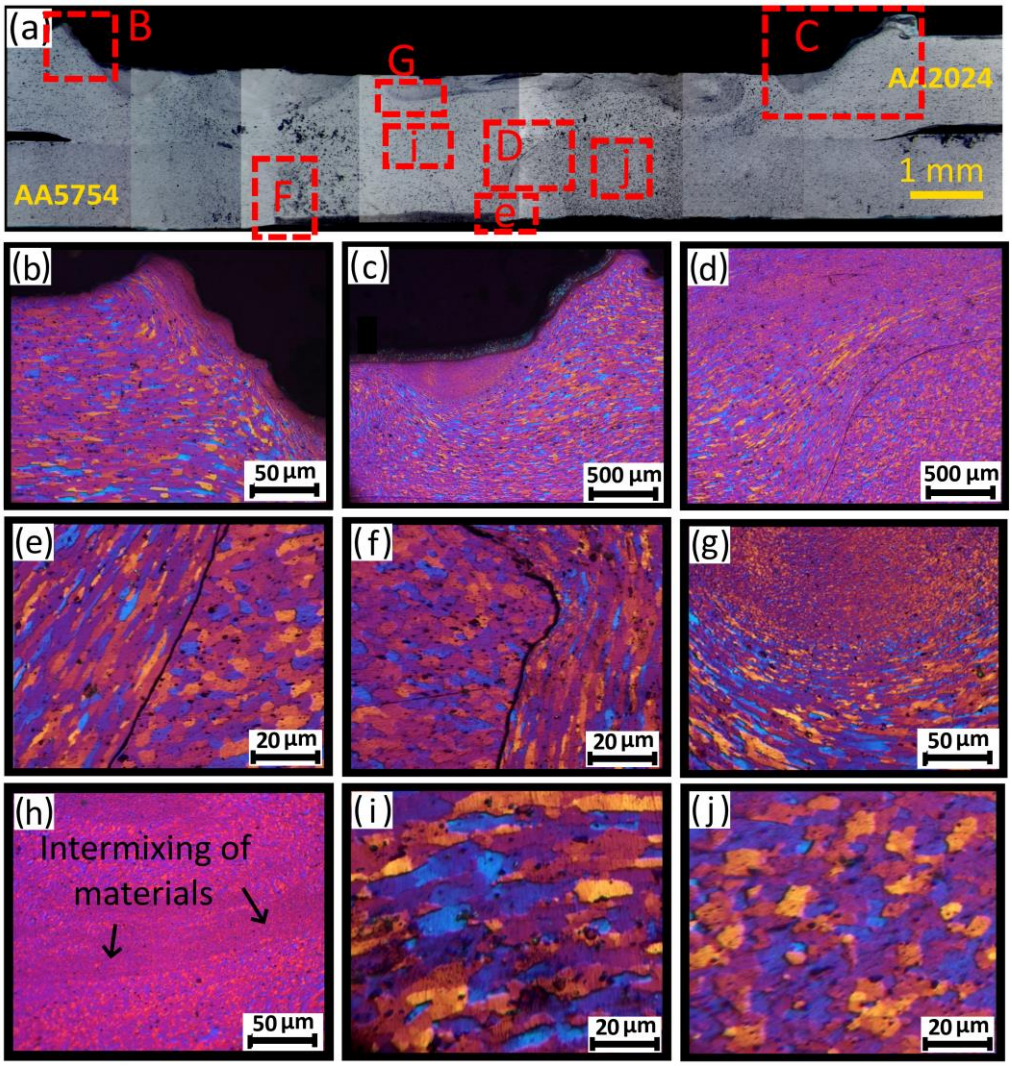

Fig. 5. Optical microstructure images of weld produced by plunge depth of 0.35 mm.

Fig: 5 (h) shows intermixing mixing between workpiece materials of AA2024-T3 and AA5754-O. This material mixing was more effectively obtained as compared to the same of region within predrilled cavity. This was because of effective forging action caused by shoulder's surface within this region that leads to more effective diffusion between workpieces. Besides, the forging was less effective at the extruded zone in the predrilled cavity, which may be the reason for forming thin separating line between workpieces at this zone, as can be seen from Fig: 5 (d), (e) and (f). Fig: 5 (i) shows SZ with recrystallized deformed grains. Fig: 5 (j) shows TMAZ with deformed grains because of higher deformation as compared to previous weld of 0.25 mm plunge depth as shown in Fig: 4 (h).

Fig. 6 shows microstructure images of weld produced by plunge depth of 0.35 mm. Increased plunge depth resulted with highest indentation as can be seen from Fig: 6 (a), as compared to previous two welds of 0.25 mm and 0.35 mm plunge depths. The metallurgical bonding of extruded material with the surfaces of predrilled cavity was more effective, as compared to previous two welds of 0.25 mm and 0.35 mm penetration depths. The oxide layer was impressively stirred and mixed in a zigzag pattern, as can be confirmed from Fig: 6 (b)-(d). In this stirred region, there is no such separating layer between AA2024-T3 and AA5754-O workpieces noticed (Fig: 6 (b)), which was observed in previous welds (Fig: 4(a) and Fig: 5 (e)-(f)). Similar effective mixing of oxide layer with zigzag pattern was observed in the stir zone region, reported in the literature of [34,35]. The stirring-plunging action was more significant in this weld of 0.45 mm penetration depth, as compared to the ones made by 0.25 mm and 0.35 mm that in turn may have resulted with effective metallurgical bonding even though thin separating oxide layer was observed. Due to strong stirring action, annular stirring patterns were noticed in ASZ as can be seen from Fig: 6 (e)-(g). The bottom surfaces of the predrilled cavity were observed with presence of thin layer of separating line between extruded material and cavity surfaces (Fig: 6 (h) and (i)), while upper portion of the same was noticed

as metallurgical bonded zone (Fig: 6 (b)-(d)). The elongated large grains were observed in the extruded zone (Fig: 6 (h) and (i)), whereas grain refinements were observed in the stirring zone with finer grain structure (Fig: 6 (b)-(d)).

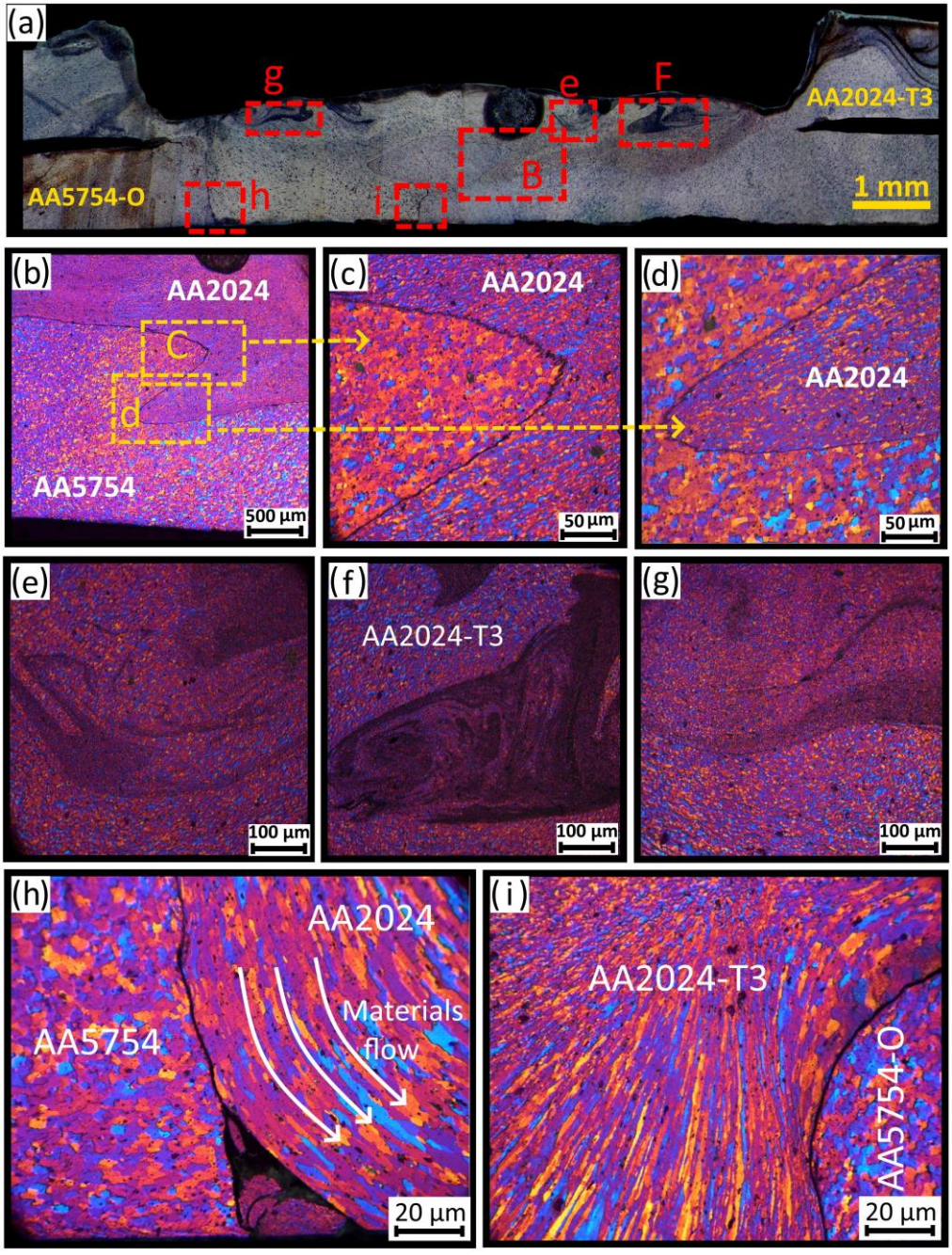

Fig. 6. Optical microstructure images of weld produced by plunge depth of 0.25 mm.

The comparative presentation of optical microstructures for different zones within single weld made by penetration depth of 0.45 mm are shown in Fig: 7. It can be seen that ASZ was observed with super refined grains (Fig: 7 (a)), wherein the stirring effect was more

pronounced. The stir zone was observed with equiaxed refined grains, but the grain size seems to be larger as compared to ASZ (Fig: 7 (b)). These grains were formed due to recrystallization caused after strong stirring action. The PDZ was consisted of elongated grains (Fig: 7 (c)) due to extrusion in the predrilled cavity. In case of TMAZ (Fig: 7 (d)-(e)) and HAZ (Fig: 7 (f)), the elongated larger grains were observed as compared to other processed zones. For TMAZ at AA2024-T3 material, the grains were elongated towards material movement downward to predrilled cavity (Fig: 7 (d)), whereas, the grains of TMAZ at AA5754-O material were consisting of horizontally elongated grains (Fig: 7 (e)). The HAZ was consisting of large grains among all the zones of processed regions. Similar microstructure zones were observed in the previous studies of [23–26].

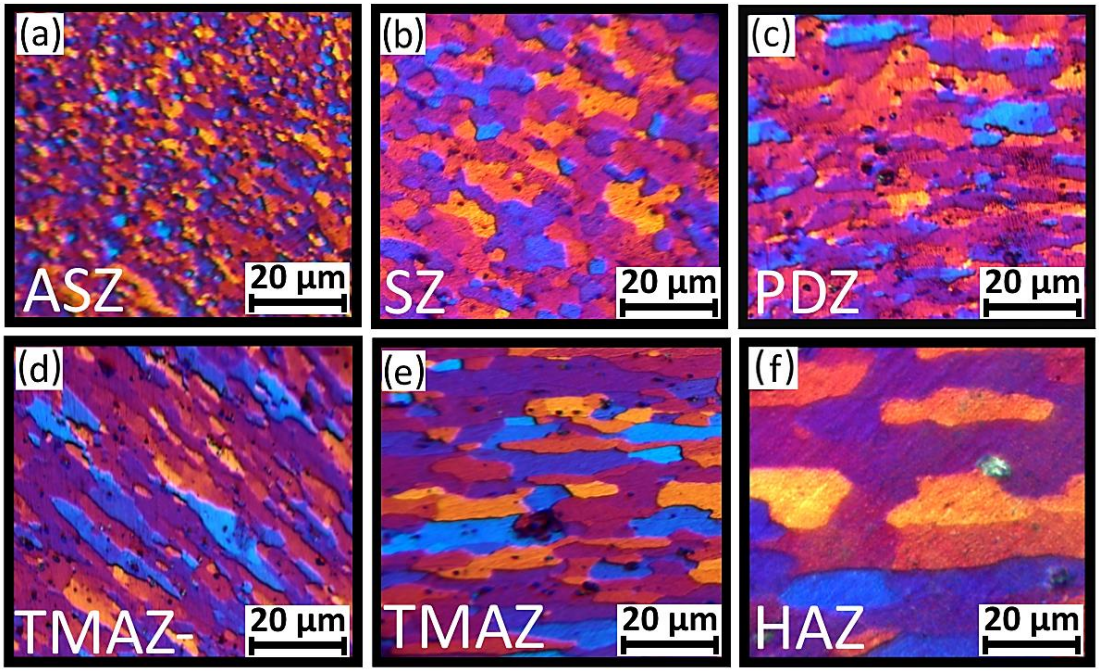

Fig. 7. Optical microstructure images of various zones for weld made by plunge depth 0.45 mm, (a) ASZ, (b) SZ, (c) PDZ, (d) TMAZ-AA2024-T3 side, (e) TMAZ-AA5754-O side, (f) HAZ.

Fig: 8 shows EBSD images of SZ and TMAZ for welds made by penetration depths of 0.25 mm and 0.45 mm. In case of 0.45 mm plunge depth, the grains of the stir zone are observed

coarser than weld made by 0.25 mm penetration depth. Also, inverse pole figure shows that majority of the grains of stir zone were oriented like [001], [111] and between [001] and [111], in case of 0.25 mm penetration depth, whereas in case of 0.45 mm penetration depth, majority of the grains of stir zone were oriented like [101], [111] and in between [101] and [111]. Similarly, TMAZ of weld produced by 0.25 mm penetration depth was consisting of finer and deformed grains, as compared to the penetration depth of 0.45 mm. Majority of the grains of TMAZ were oriented like in between [001] and [111] in case of 0.25 mm penetration depth, whereas the same were oriented like in between [001] and [101] in case of 0.45 mm penetration depth.

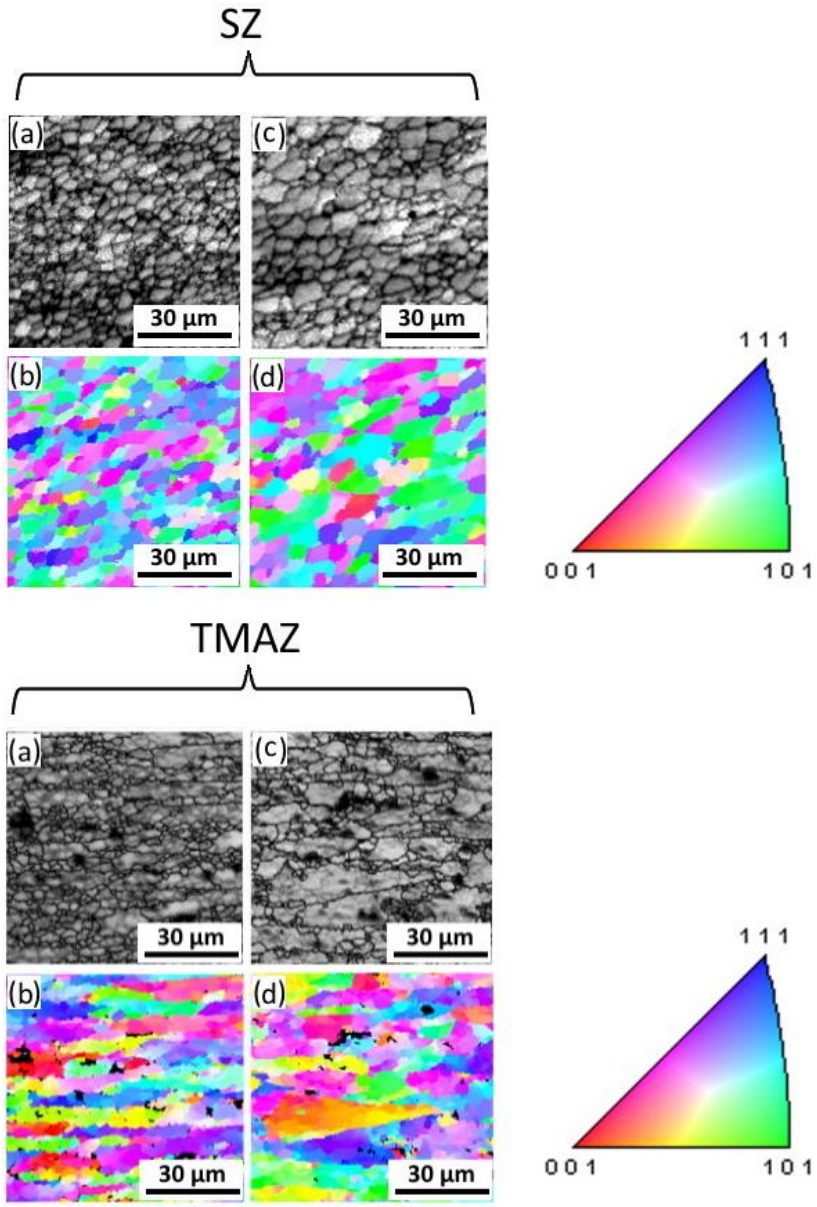

Fig. 8. EBSD iamges of stir zone and TMAZ for welds made by penetration depth of (a) and (b) 0.25 mm, and (c) and (d) 0. 45 mm.

The evidences of materials mixing at the interface between extruded material and predrilled cavity material within the stir zone region are shown in Fig: 9. Fig: 9 (a) and (b) show intermexing (with interlocking) between materials AA2024-T3 and AA5754-O for the weld produced by 0.25 mm penetration depth. In this weld speciemen, distinct interface was appeared between both the materials, however, mechanical interlocking between both the workpiece materials was also evidenced. On the other hand, no disctinct interface was observed in case of weld produced by 0.45 mm penetration depth as can be seen from Fig: 9 (c) and (d).

In this case, enhanced stirring patterns with effective bonding can be seen from Fig: 9 (c) and (d).

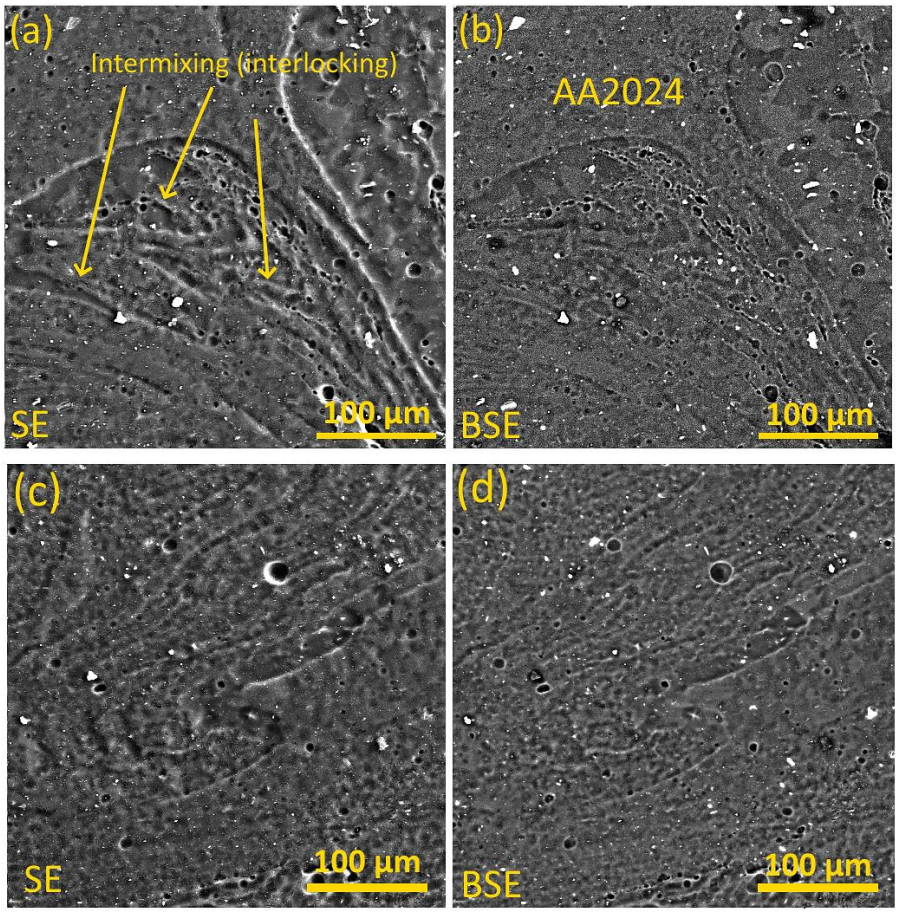

Fig. 9. SEM images of welds, (a) and (b) 0.25 mm, (c) and (d) 0.45 mm.

3.3. Tensile testing

The tensile testing results are shown in Fig: 10; wherein fractured load vs shoulder plunge depth (penetration depth) is represented in Fig: 10 (a), macrographs of fracture location is represented in Fig: 10 (b) and SEM of fractured surfaces is represented in Fig: 10 (c). It can be seen from Fig: 10 (a) that the maximum fracture load of 5198 N was observed in the weld made by penetration depth of 0.45 mm, whereas minimum fracture load of 2136 N was observed in the weld made by penetration depth of 0.25 mm. Enhanced metallurgical bonding was observed and discussed in case of weld made by penetration depth of 0.45 mm that resulted into higher fracture load, which can be confirmed from fractured specimen (Fig: 10 (c)). In this, the specimen was fractured from TMAZ side. Although, this weld was consisting of higher

indentation, the failure was occurred from TMAZ and not from cavity of indentation. It shows better metallurgical bonding. However, geometrical inhomogeneity with higher indentation increases the chances of failure during loading in service [24]. Therefore, plunging depth must be optimized for indentation and metallurgical bonding. Besides, weld of 0.25 mm penetration depth was observed with less effective metallurgical bonding and therefore, it was resulted with lower fractured load. Also, the welded specimen was detached from the interface between extruded material and surfaces of predrilled cavity during tensile testing (Fig: 10 (b)).

The fractured surfaces after tensile testing as analyzed by SEM as shown in Fig: 10 (d) for the weld of 0.45 mm penetration depth. It can be confirmed that the fracture was occurred from the TMAZ near to the interface between workpieces. It can be seen that majority of the fractured surfaces were consisting of dimples. This indicates inter-granular fracture mode of ductile fracture behavior. In some regions of fractured surface images, full grains and flat surfaces were observed, which were from mechanically interlocked region. In these regions, it can be said that the metallurgical bonding with materials intermixing was not effective. The investigation on peripheral bonding between the cavity of predrilled surfaces and extruded material may provide more details on mixed details of metallurgical bonded regions and mechanically interlocked regions within the periphery of processed region.

4. Conclusions

Friction spot extrusion welding was investigated for dissimilar AA2024-T3 and AA5754-O materials with three different plunge depths, keeping other process parameters constant. Following conclusions can be made based on this investigation.

(1) In friction spot extrusion welding, optimum plunge depth is required to obtain enhanced metallurgical bonding between extruded material and surfaces of predrilled cavity in

addition to mechanical interlocking. Plunge depth of 0.25 mm was resulted with only mechanical locking of extruded material in the predrilled cavity without any strong evidence on metallurgical bonding. Plunge depth of 0.45 mm was resulted with effective metallurgical bonding between extruded material and surfaces of predrilled cavity in addition to mechanical locking of extruded material in the predrilled cavity.

(2) Different microstructures such as stir zone, annular stir zone, extruded zone, thermo-mechanically affected zone and heat affected zone were noticed with variations in grain size and features. Change in plunge depth influences grain structure of different processed zones.

(3) Increased plunge depth of 0.45 mm resulted in effective stirring-plunging with zigzag mixing of oxide layer in the processed zone. In case of plunge depth of 0.25 mm, separating oxide layer was observed between both the workpieces.

(4) The weld produced by maximum plunge depth of 0.45 mm (among three investigated) fractured with higher load of 5198 N during tensile testing. Trans-granular ductile fracture mode was majorly observed, in case of weld produced by plunge depth of 0.45 mm.

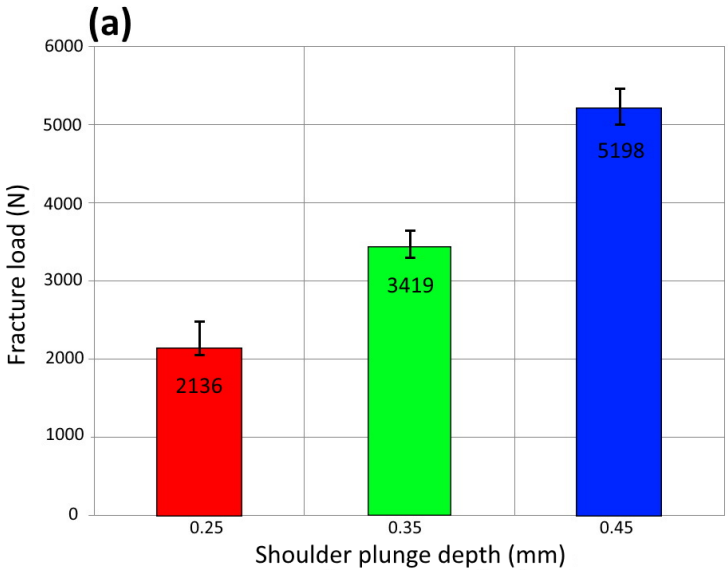

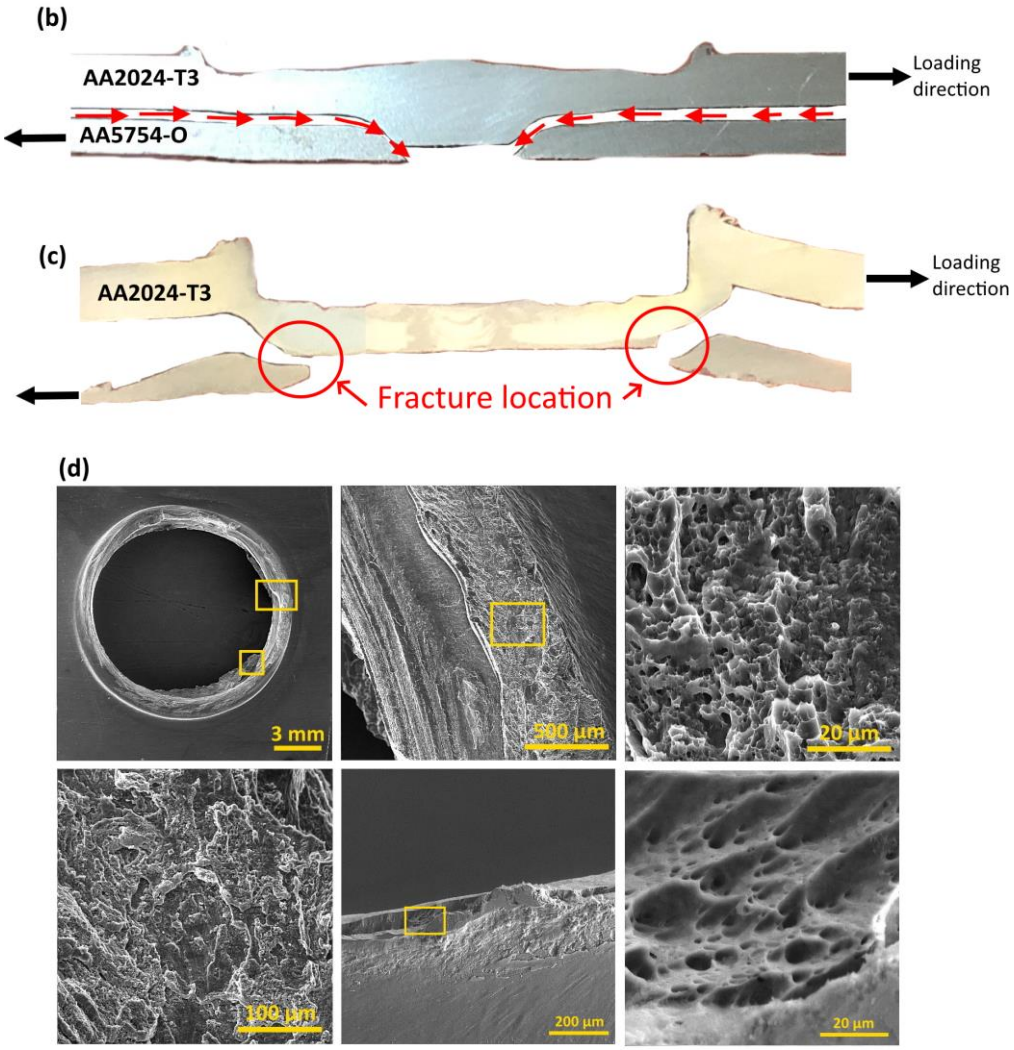

Fig. 10. Tensile testing results, (a) fractured load after tensile testing, (b) fracture location of weld of penetration depth 0.25 mm, (c) fracture location of weld of penetration depth 0.45 mm, and (d) SEM images of fractured surfaces.

References

[1] Martinsen K, Hu SJ, Carlson BE. Joining of dissimilar materials. CIRP Ann - Manuf Technol 2015;64:679–99. https://doi.org/10.1016/j.cirp.2015.05.006.

[2] Haghshenas M, Gerlich AP. Joining of automotive sheet materials by friction-based welding methods: A review. Eng Sci Technol an Int J 2018;21:130–48. https://doi.org/10.1016/j.jestch.2018.02.008.

[3] Thomas W., Nicholas E. Friction stir welding for the transportation industries. Mater Des 1997;18:269–73. https://doi.org/10.1016/S0261-3069(97)00062-9.

[4] Mehta KP. A review on friction-based joining of dissimilar aluminum-steel joints. J Mater Res 2019;34:78–96. https://doi.org/10.1557/jmr.2018.332.

[5] Mehta KP, Badheka VJ. A review on dissimilar friction stir welding of copper to

aluminum: Process, properties, and variants. Mater Manuf Process 2016;31:233–54. https://doi.org/10.1080/10426914.2015.1025971.

[6] Mehta KP, Carlone P, Astarita A, Scherillo F, Rubino F. Conventional and cooling assisted friction stir welding of AA6061 and AZ31B alloys. Mater Sci Eng A 2019;759:252–61. https://doi.org/10.1016/j.msea.2019.04.120.

[7] Vyas HD, Mehta KP, Badheka V, Doshi B. Processing and evaluation of dissimilar Al-SS friction welding of pipe configuration: Nondestructive inspection, properties, and microstructure. Meas J Int Meas Confed 2021;167:108305. https://doi.org/10.1016/j.measurement.2020.108305.

[8] Patel NP, Parlikar P, Dhari RS, Mehta K, Pandya M. Numerical modelling on cooling assisted friction stir welding of dissimilar Al-Cu joint. J Manuf Process 2019;47:98–109. https://doi.org/10.1016/j.jmapro.2019.09.020.

[9] Paidar M, Ojo OO, Moghanian A, Pabandi HK, Elsa M. Pre-threaded hole friction stir spot welding of AA2219 / PP-C30S sheets. J Mater Process Tech 2019;273:116272. https://doi.org/10.1016/j.jmatprotec.2019.116272.

[10] Shen Z, Ding Y, Gerlich AP. Advances in friction stir spot welding. Crit Rev Solid State Mater Sci 2019;0:1–78. https://doi.org/10.1080/10408436.2019.1671799.

[11] Pan TY. Friction stir spot welding (FSSW) - A literature review. SAE Tech Pap 2007;2007. https://doi.org/10.4271/2007-01-1702.

[12] Mehta KP, Patel R. On fsw keyhole removal to improve volume defect using pin less tool. Key Eng Mater 2019;821 KEM:215–21. https://doi.org/10.4028/www.scientific.net/KEM.821.215.

[13] Mehta KP, Patel R, Vyas H, Memon S, Vilaça P. Repairing of exit-hole in dissimilar Al-Mg friction stir welding: Process and microstructural pattern. Manuf Lett 2020;23:67–70. https://doi.org/10.1016/j.mfglet.2020.01.002.

[14] Huang YX, Han B, Tian Y, Liu HJ, Lv SX, Feng JC, et al. New technique of filling friction stir welding. Sci Technol Weld Join 2011;16:497–501. https://doi.org/10.1179/1362171811Y.0000000032.

[15] Behmand SA, Mirsalehi SE, Omidvar H, Safarkhanian MA. Filling exit holes of friction stir welding lap joints using consumable pin tools. Sci Technol Weld Join 2015;20:330–6. https://doi.org/10.1179/1362171815Y.0000000018.

[16] Xu Z, Li Z, Ji S, Zhang L. Refill friction stir spot welding of 5083-O aluminum alloy. J Mater Sci Technol 2018;34:878–85. https://doi.org/10.1016/j.jmst.2017.02.011.

[17] Reimann M, Goebel J, dos Santos JF. Microstructure and mechanical properties of keyhole repair welds in AA 7075-T651 using refill friction stir spot welding. Mater Des 2017;132:283–94. https://doi.org/10.1016/j.matdes.2017.07.013.

[18] Reimann M, Goebel J, Gartner TM, dos Santos JF. Refilling termination hole in AA 2198–T851 by refill friction stir spot welding. J Mater Process Technol 2017;245:157–66. https://doi.org/10.1016/j.jmatprotec.2017.02.025.

[19] Paidar M, Ghavamian S, Ojo OO, Khorram A, Shahbaz A. Modified friction stir clinching of dissimilar AA2024-T3 to AA7075-T6: Effect of tool rotational speed and penetration depth. J Manuf Process 2019;47:157–71. https://doi.org/10.1016/j.jmapro.2019.09.028.

[20] Paidar M, Ojo OO, Moghanian A, Karapuzha AS, Heidarzadeh A. Modified friction stir clinching with protuberance-keyhole levelling: A process for production of welds with high strength. J Manuf Process 2019;41:177–87. https://doi.org/10.1016/j.jmapro.2019.03.030.

[21] Haiyan Z, Mehta KP. Effect of materials positioning on dissimilar modified friction stir clinching between aluminum 5754-O and 2024-T3 sheets. Vacuum 2020;178:109445. https://doi.org/10.1016/j.vacuum.2020.109445.

[22] Gao P, Zhang Y, Mehta KP. Metallurgical and Mechanical Properties of Al–Cu Joint by Friction Stir Spot Welding and Modified Friction Stir Clinching. Met Mater Int 2020. https://doi.org/10.1007/s12540-020-00759-w.

[23] Han J, Paidar M, Vignesh RV, Mehta KP, Heidarzadeh A, Ojo OO. Effect of shoulder features during friction spot extrusion welding of 2024-T3 to 6061-T6 aluminium alloys. Arch Civ Mech Eng 2020;20:84. https://doi.org/10.1007/s43452-020-00086-2.

[24] Saju TP, Narayanan RG. Dieless friction stir extrusion joining of aluminum alloy sheets with a pinless stir tool by controlling tool plunge depth. J Mater Process Technol 2020;276:116416. https://doi.org/10.1016/j.jmatprotec.2019.116416.

[25] Saju TP, Narayanan RG. Dieless friction stir lap joining of AA 5050-H32 with AA 6061-T6 at varying pre-drilled hole diameters. J Manuf Process 2020;53:21–33. https://doi.org/10.1016/j.jmapro.2020.01.048.

[26] Saju TP, Narayanan RG, Roy BS. Effect of pinless tool shoulder diameter on dieless friction stir extrusion joining of AA 5052-H32 and AA 6061-T6 aluminum alloy sheets. J Mech Sci Technol 2019;33:3981–97. https://doi.org/10.1007/s12206-019-0136-1.

[27] Zhang G ju, Xiao C yuan, Ojo OO. Dissimilar friction stir spot welding of AA2024-T3/AA7075-T6 aluminum alloys under different welding parameters and media. Def Technol 2020;6. https://doi.org/10.1016/j.dt.2020.03.008.

[28] Suryanarayanan R, Sridhar VG. Effect of Process Parameters in Pinless Friction Stir Spot Welding of Al 5754-Al 6061 Alloys. Metallogr Microstruct Anal 2020;9:261–72. https://doi.org/10.1007/s13632-020-00626-5.

[29] Da Silva AM, Aldanondo E, Olaran I, Alvarez P, Echeverria A. Effect of joining

parameters on performance of similar and dissimilar AA5754-H22 and AA6082-T6 friction stir spot welded aluminium alloys. SAE Tech Pap 2010. https://doi.org/10.4271/2010-01-1155.

[30] Gerlich A, Yamamoto M, North TH. Local melting and tool slippage during friction stir spot welding of Al-alloys. J Mater Sci 2008;43:2–11. https://doi.org/10.1007/s10853-007-1791-7.

[31] Bozkurt Y, Salman S, Çam G. Effect of welding parameters on lap shear tensile properties of dissimilar friction stir spot welded aa 5754-h22/2024-t3 joints. Sci Technol Weld Join 2013;18:337–45. https://doi.org/10.1179/1362171813Y.0000000111.

[32] Lazarevic S, Ogata KA, Miller SF, Kruger GH, Carlson BE. Formation and structure of work material in the friction stir forming process. J Manuf Sci Eng Trans ASME 2015;137:1–9. https://doi.org/10.1115/1.4030641.

[33] Oladimeji OO, Taban E, Kaluc E. Understanding the role of welding parameters and tool profile on the morphology and properties of expelled flash of spot welds. Mater Des 2016;108:518–28. https://doi.org/10.1016/j.matdes.2016.07.013.

[34] Okamura H, Aota K, Sakamoto M, Ezumi M, Ikeuchi K. Behaviourof oxides during friction stir welding of aluminium alloy and their effect on its mechanical properties. Weld Int 2002;16:266–75. https://doi.org/10.1080/09507110209549530.

[35] Buffa G, Campanella D, Fratini L. On tool stirring action in friction stir welding of work hardenable aluminium alloys. Sci Technol Weld Join 2013;18:161–8. https://doi.org/10.1179/174329312X13559959303691.